Daisy: A Large Flexible Space Structure Testbed for Advanced Control Experiments

Benoit Boulet[1]*, *Bruce A. Francis*[1]**, *Peter C. Hughes*[2], *and Tony Hong*[2]

[1] Electrical and Computer Engineering, University of Toronto, Toronto, Ont., Canada M5S 1A4.

[2] Institute for Aerospace Studies, University of Toronto, 4925 Dufferin Street, North York, Ont., Canada M3H 5T6.

1 Introduction

Daisy is an experimental testbed facility at the University of Toronto's Institute for Aerospace Studies (UTIAS) whose dynamics are meant to emulate those of a real large flexible space structure (LFSS); see Figure 1 [8]. The purpose of the facility is to test advanced identification and multivariable control design methods. Modeled roughly to resemble the flower of the same name, Daisy consists of a rigid hub (the "stem") mounted on a spherical joint and on top of which are ten ribs (the "petals") attached through passive two-degree-of-freedom rotary joints and low-stiffness springs. Each rib is coupled to its two neighbors via low-stiffness springs. The hub would represent the rigid part of a LFSS, while the ribs would model its flexibilities.

Concerning Daisy's actuators, each rib is equipped with four unidirectional air jet thrusters that are essentially on-off devices, each capable of delivering a torque of 0.8 Nm at the rib joint. Pulse-width modulation (PWM) of the thrust is used to apply desired torques on the ribs. The four thrusters are aligned by pairs to implement two orthogonal bidirectional actuators. The hub actuators consist of three torque wheels driven by DC motors whose axes are orthogonal. Each can deliver up to 38.8 Nm.

Concerning the sensors, mounted at the tip of each rib is an infra-red emitting diode. Two hub-mounted infra-red CCD cameras measure the positions of these diodes via ten lenses. The cameras are linked to a computer that from the kinematics of Daisy computes the 20 rib angles relative to the hub in real-time (at a 30 Hz sampling rate) from the sampled infra-red video frames. This vision system, called DEOPS (Digital Electro-Optic Position Sensor), was developed at UTIAS [17]. Its resolution is approximately 0.1% of the cameras' field of view, which roughly translates to an angle measurement accuracy of 3.5×10^{-4} radians (0.02 degrees) in the ideal case. The hub orientation and angular velocity can be

* Supported through scholarships from the Natural Sciences and Engineering Research Council (NSERC) of Canada, the Fonds pour la formation de chercheurs et l'aide à la recherche, Québec, and a Walter C. Sumner Memorial Fellowship.

** Supported by NSERC.

measured with position and velocity encoders. There are also accelerometers on the ribs, but for this research only DEOPS and the hub position encoders were used as sensors.

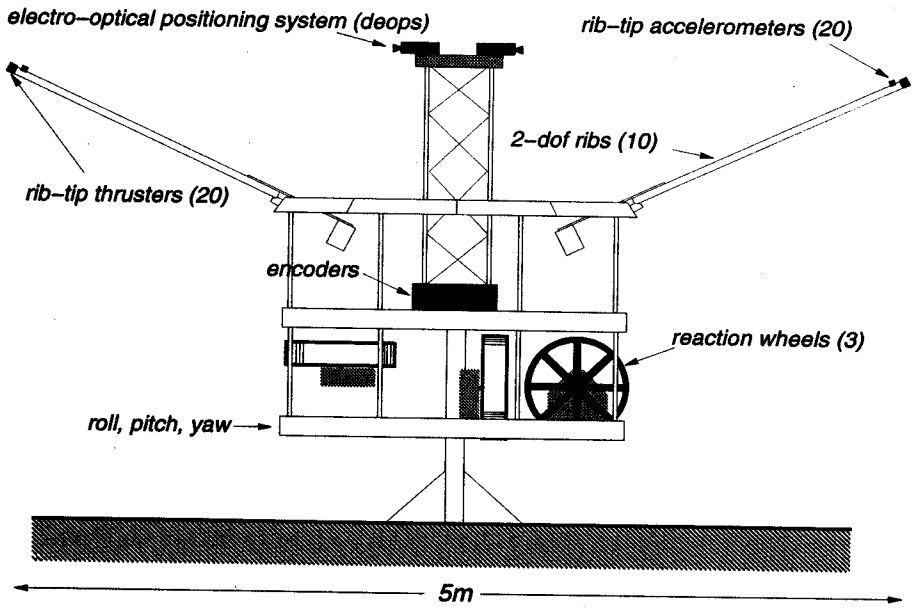

Fig. 1. Daisy LFSS experimental testbed.

In general, the dynamics of LFSSs are characterized by their high order and their significant number of closely-spaced, lightly-damped, clustered low-frequency modes. They pose a challenging problem to the control system designer, who must deal with those characteristics while ensuring a certain level of robustness in the face of significant model uncertainty. Mathematical linear dynamic models of LFSSs are usually obtained using finite-element (FE) methods, but these models are known to be accurate only for the first few modes of the structure. Moreover, these models do not provide the modal damping ratios, hence they are originally undamped. Model identification of LFSSs is often impractical because such structures are assembled in space and cannot be easily tested on earth due to problems caused by the gravity field and the atmosphere. Thus it would be desirable to have a design procedure that would directly use an FE model and a natural description of the uncertainty to produce a controller that could be implemented on real LFSSs with good confidence.

Daisy is a challenging testbed for the following reasons:

–The dynamic model available for Daisy is linear, of order 46, including 20 flexible modes and three rigid-body modes. The natural frequencies of the flexible modes are clustered around 0.6 rad/s, and model reduction is not possible, at least by conventional methods. An order of 46 presents a challenge, both for controller design and for subsequent digital implementation.
–There is significant uncertainty in modal parameters, for example, up to 50% uncertainty in damping constants.
–Daisy has some pronounced nonlinear characteristics, the most prominent being the PWM mode of the air-jet thrusters, together with their reaction delay.

Our program of research on Daisy includes the following issues:

–Getting a non-conservative linear uncertainty model.
–Testing the applicability of $\mathcal{H}_\infty$ optimization to control design for Daisy, and LFSSs in general.
–Developing a method for model validation.
–Testing the applicability of μ optimization.
–Testing the applicability of recent optimal sampled-data methods.
–Studying the control of Daisy with non-colocation, that is, without a full complement of actuators and sensors.
–Developing an effective tool for PWM control in the H-inf framework.

This paper summarises our results on the first two items. For a more complete report, the reader is referred to [4].

Notation

The norm of a complex matrix is taken to be its maximum singular value: $\|H\| = \overline{\sigma}(H)$. The ∞-norm of x in $\mathbb{R}^n$ is $\|x\|_\infty = \max_{i=1,\ldots,n} |x_i|$. We denote the open and closed right-half complex planes by $\mathbb{C}_+$ and $\overline{\mathbb{C}}_+$ respectively. The extension of $\overline{\mathbb{C}}_+$ to infinity is written as $\overline{\mathbb{C}}_+ \cup \{\infty\}$. For a normed space $\mathcal{X}$, $\mathcal{B}\mathcal{X}$ denotes its open unit ball.

2 Modeling LFSSs

Uncertainty modeling in LFSSs is critical if one is to achieve an acceptable level of robustness with a practical controller. Some works [19], [1], [25] use norm-bounded additive or multiplicative perturbations of a nominal model in the frequency domain to account for uncertainty in the modal frequencies, damping ratios, and mode shape matrix of the model. Unmodeled modes of the structure and uncertain actuator dynamics can also be represented in this way [20]. Such approaches to uncertainty modeling in LFSSs do not handle modal parameter uncertainty very well: Slight variations in either the mode frequencies or damping

ratios usually cause the associated dynamic perturbations to be large in the ∞-norm sense. Indeed, additive or multiplicative perturbations may contain large peaks in their frequency responses because of the inherently low damping ratios in LFSS dynamics. At the limit, undamped modes cannot have a representation as norm-bounded perturbations of these types. Covering unmodeled modes with such perturbations suffers from the same problem. As a result, one has to choose large weighting functions to bound perturbations that arise from small variations in the modal parameters. In an actual $\mathcal{H}_\infty$ controller design, this may lead to difficulties in making the closed-loop system robustly stable to all weighted perturbations of admissible ∞-norm while achieving some desired performance objective. Thus, in this case, the basic tradeoff between robust stability and nominal performance may be detrimental to the achievable performance level.

In this paper, it is suggested to transform real parameter uncertainty in the modes into unstructured uncertainty without getting too conservative in the sense that the uncertainty set in $\mathcal{H}_\infty$ has to be kept relatively small. This is motivated by the fact that many results and practical controller design techniques are available for this kind of uncertainty, whereas a useful frequency-based design method dealing explicitly with a large number of scalar real structured perturbations in a high-order dynamic model has yet to be developed. So far, μ-synthesis has proven to be one of the most effective ways to deal with complex structured uncertainty, and some authors (e.g. [19]) have used it to model real parametric uncertainty. Recently the mixed real/complex μ problem has been studied [11] and design methods based on minimizing an upper bound on the mixed μ function, such as the so-called Popov controller synthesis [14], have been developed. Application to a flexible structure has been reported in [15]. These methods are attractive but they quickly become numerically difficult (actually, they are NP-hard [5]) as the plant's order and the number of independent perturbations increase. Some of them also suffer from controller inflation. Hence they are of limited use for high-order LFSS models when many real scalar perturbations are modeled as individual scalar blocks. Furthermore, an unstructured complex uncertainty block must still be added to account for unmodeled dynamics, and this block usually represents additive or multiplicative uncertainty. This means that the attainable performance may be severely limited as previously discussed.

Yet another approach to the robust control of LFSSs is the passivity approach [16]. It is well known that an LFSS with colocated rate sensors and force/torque actuators and with the same number of inputs and outputs has a positive-real transfer matrix model. Then if a strictly positive real controller is designed, it follows that the closed-loop will be stable for all modal perturbations, regardless of the number of unmodeled modes. Although this result is of great importance, it only applies to structures of rather restricted configurations. Moreover, one cannot use this result for controller design achieving robust performance. Recently, dynamic embeddings have been proposed to turn a nonsquare/noncolocated LFSS model into a positive real system [18]. Even though this approach seems promising, it is not yet clearly known how robust the embedding technique is, i.e., small perturbations in the original plant may destroy

the positive realness property of the embedded plant.

It appears that a different description of the uncertainty is needed. Some authors have argued (e.g. [26]) that coprime factor descriptions in $\mathcal{H}_\infty$ of nearly unstable plants, such as LFSSs, is a sound way to model these systems. This is the approach taken here, as introduced in [3]. The loopshaping technique of McFarlane and Glover [21] involves modeling the plant as a normalized coprime factorization and it has been successfully applied to design controllers for LFSSs [21]. Similar to the loopshaping method is the weighted-gap optimization technique that was tested on LFSS experimental facilities by Buddie et al. [6]. These techniques show the potential of modeling LFSS dynamics using coprime factorizations, but they don't address the problem of converting known bounds on perturbations of the modal parameters into norm bounds on factor perturbations. The difficulty comes from the fact that these methods rely on *normalized* coprime factorizations, which destroy the decoupled structure of the nominal modal state-space models.

Section 3 presents a very simple method to obtain a left coprime factorization (LCF) of LFSS dynamics in modal coordinates that preserves the decoupled structure. The plant uncertainty is described as stable perturbations of the coprime factors. The structure of the LCF allows one to go easily from modal parameter uncertainty to an unstructured description of the uncertainty as stable norm-bounded perturbations in the factors, as discussed in Section 4. This allows a better, less conservative description of the uncertainty set and hence should lead to better closed-loop performance and guaranteed robustness.

3 A Left Coprime Factorization of LFSS Dynamics

An FE method gives a high-order model of the flexible part of the structure consisting of perhaps thousands of ordinary differential equations. Rigid-body modes may be included to account for the attitude and position of rigid parts of the structure. In order to have a fixed model for our discussion, we consider three rigid-body modes accounting for the attitude of the main rigid part. (Daisy has these dynamics, although two of the rigid-body modes are pendulous, so they can be viewed as flexible modes.) The model is undamped, and it consists essentially of a positive definite mass matrix M and a positive semidefinite stiffness matrix K; the equations are

$$M\ddot{q} + Kq = B_0 u \tag{1}$$

$$y = C_0 q, \tag{2}$$

where $q(t) \in \mathbb{R}^{n_{FE}}$ is a vector of attitude coordinates for the rigid part and physical coordinates (displacements and rotations) of the flexible parts of the LFSS, the input $u(t) \in \mathbb{R}^m$ is a vector of actuator forces and torques applied to the structure, and $y(t) \in \mathbb{R}^p$ is the vector of measured outputs.

A real matrix E whose columns are eigenvectors of the matrix $M^{-1}K$ and such that it diagonalizes both M and K, i.e., $E^T M E = I$ and $E^T K E = \Lambda$,

where Λ is diagonal with the squared mode frequencies on its main diagonal, always exists ([13], Theorem 4.5.15). It defines a coordinate transformation from the modal coordinate vector η to the physical coordinate vector q, i.e., $q = E\eta$. Such a matrix is called a *mode shape matrix* of the system and its columns are the *mode shapes* of the structure. Thus the mode shapes and mode frequencies are the eigenvectors and eigenvalues of $M^{-1}K$.

We start with LFSS dynamics in modal coordinates, reduced to a reasonable order by discarding the less significant flexible modes according to some measure of their input-output influence [24], [12]. The first three are the rigid-body modes. The modal frequencies of the $n-3$ remaining retained flexible modes, $\{\omega_i\}_{i=4}^n$, are given by the FE model; uncertainties will be introduced later. Damping is added to the nominal model, as it is known that damping ratios of flexible modes are nonzero, since flexibilities in any LFSS are dissipative in nature. So if $\{\overline{\zeta}_i\}_{i=4}^n$ are positive upper bounds and $\{\underline{\zeta}_i\}_{i=4}^n$ nonnegative lower bounds on the otherwise unknown damping ratios, we may take $\{\zeta_i := (\underline{\zeta}_i + \overline{\zeta}_i)/2\}_{i=4}^n$ as the nominal ones. Transforming (1) using the mode shape matrix E, truncating, and adding a diagonal damping matrix D, we get the nominal dynamic equations in modal coordinates:

$$\ddot{\eta} + D\dot{\eta} + \Lambda\eta = B_1 u \tag{3}$$

$$y = C_1\eta, \tag{4}$$

where

$$\begin{aligned} D &= \mathrm{diag}\{0,0,0,2\zeta_4\omega_4,\ldots,2\zeta_n\omega_n\} \\ \Lambda &= \mathrm{diag}\{0,0,0,\omega_4^2,\ldots,\omega_n^2\} \\ B_1 &= E_r^T B_0 \\ C_1 &= C_0 E_r \end{aligned}$$

and E_r is composed of the columns of E corresponding to the modes kept in the model. Thus

$$\hat{\eta}(s) = [s^2 I + sD + \Lambda]^{-1} B_1 \hat{u}(s) \tag{5}$$

$$\hat{y}(s) = C_1 [s^2 I + sD + \Lambda]^{-1} B_1 \hat{u}(s). \tag{6}$$

The assumptions here are as follows:

(A1) The sensors have no dynamics.

(A2) No pole-zero cancellation at $s = 0$ occurs when the product $C_1 [s^2 I + sD + \Lambda]^{-1} B_1$ is formed.

(A3) The uncertainty in the output matrix C_1 can be lumped in with the input uncertainty.

The motivation behind assumptions (A1) and (A3) is that space sensors are usually accurate and fast while space actuators, which include torque wheels and gas jet thrusters, may add quite a bit of uncertainty in the torque and force inputs. Assumption (A2) is standard and just says that the unstable rigid-body

modes must be controllable and observable with the set of actuators and sensors used.

Consider the matrix $[s^2 I + sD + \Lambda]$ in (5). It is diagonal, so its inverse is simply

$$[s^2 I+sD+\Lambda]^{-1} = \text{diag}\left\{\frac{1}{s^2}, \frac{1}{s^2}, \frac{1}{s^2}, \frac{1}{s^2+2\zeta_4\omega_4 s+\omega_4^2}, \ldots, \frac{1}{s^2+2\zeta_n\omega_n s+\omega_n^2}\right\}. \tag{7}$$

The matrix B_1 in (5) is an $n \times m$ real matrix. Introduce a polynomial s^2+as+b, Hurwitz with real zeros, and form the matrices $\tilde{M}(s)$, $\tilde{N}(s)$ as follows:

$$\tilde{M}(s) := \frac{1}{s^2+as+b}\text{diag}\left\{s^2, s^2, s^2, s^2+2\zeta_4\omega_4 s+\omega_4^2, \ldots, s^2+2\zeta_n\omega_n s+\omega_n^2\right\} \tag{8}$$

$$\tilde{N}(s) := \frac{1}{s^2+as+b}B_1. \tag{9}$$

The complex argument s is dropped hereafter to ease the notation. Note that $\tilde{M}$ and $\tilde{N}$ belong to $\mathcal{RH}_\infty$ and the transfer function matrix from $\hat{u}$ to $\hat{\eta}$ is $G := \tilde{M}^{-1}\tilde{N}$, i.e., $\tilde{M}$ and $\tilde{N}$ form a left factorization of G in $\mathcal{RH}_\infty$. It can be proved that $\tilde{M}$ and $\tilde{N}$ are left coprime.

4 Uncertainty Modeling for LFSSs

Uncertainty in FE models is usually characterized by uncertainty in the modal parameters $\{\zeta_i\}_{i=4}^n$ and $\{\omega_i\}_{i=4}^n$, in the mode gains, and in the mode shape matrix E. Unmodeled modes can also be considered as perturbations changing the order of the model. Uncertainty in the modal parameters appears easier to characterize based on heuristics and experience, at least for the first few modes, than uncertainty in E. The uncertainty modeling process proposed here uses the a priori knowledge of the bounds for $\{\zeta_i\}_{i=4}^n$, $\{\omega_i\}_{i=4}^n$. For example, the structure designer might say with good certainty that the second mode has natural frequency between, say, 0.01 and 0.013 rd/s, and that its damping ratio ζ is almost surely less than 0.05. This information is used to derive a bound on the norm of the coprime factor perturbations at each frequency, which will be needed in the design process for robustness issues. Of course, some uncertainty is also present in the mode shape matrix E of the structure and will be accounted for as uncertainty in the entries of B_1. We will see that it is easy to go from parametric uncertainty to unstructured uncertainty in the coprime factors.

This section can be outlined as follows. First we start with the parametric uncertainty model (11); this induces stable perturbations in $\tilde{M}$ and $\tilde{N}$. These induced perturbations and their corresponding perturbed factors are given the subscript "*rp*" for *real parameter*. On the other hand, some of the results stated apply to more general perturbations in $\mathcal{RH}_\infty$, but then the subscript is dropped. Two scalings are performed on $\tilde{M}_{rp}$ and $\tilde{N}_{rp}$ so that the perturbations are better balanced. Finally, a third scaling normalizes the combined factor perturbations.

It is desired to lump the uncertainty in the mode frequencies, damping ratios, and mode gains into unstructured uncertainty in the coprime factors such that the perturbed LCF of $\boldsymbol{G}$ can be written as

$$\boldsymbol{G}_p = (\tilde{\boldsymbol{M}} + \Delta\boldsymbol{M})^{-1}(\tilde{\boldsymbol{N}} + \Delta\boldsymbol{N}), \tag{10}$$

with $\Delta\boldsymbol{M}$, $\Delta\boldsymbol{N} \in \mathcal{RH}_\infty$. Perturbations in the modal parameters and the entries of B_1 are assumed bounded by nonnegative numbers as follows:

$$|\delta\omega_i| \le l_\omega^i\ , \quad |\delta\zeta_i| \le l_\zeta^i\ , \quad |\delta b_{1ij}| \le l_b^{ij}\ , \quad i,j = 1,\ldots,n. \tag{11}$$

The following matrices will be useful later on:

$$\Delta B_1 := \begin{bmatrix} \delta b_{11} & \cdots & \delta b_{1m} \\ \vdots & \ddots & \vdots \\ \delta b_{n1} & \cdots & \delta b_{nm} \end{bmatrix} \tag{12}$$

$$L_B := \begin{bmatrix} l_b^{11} & \cdots & l_b^{1m} \\ \vdots & \ddots & \vdots \\ l_b^{n1} & \cdots & l_b^{nm} \end{bmatrix}. \tag{13}$$

The uncertainty in the entries of B_1, which are also the numerators of the fractional entries of $\tilde{\boldsymbol{N}}$, comes from different sources. First, uncertainty in a particular mode gain can be represented as an uncertain factor multiplying the corresponding row of B_1. Second, uncertainty in the mode shape matrix E affects B_1 because in the change from physical to modal coordinates in (1), the original input matrix B_0 gets premultiplied by E_r^T to form B_1. Third, the matrix B_0 itself is uncertain because the actuator gains are not known perfectly. Finally, by (A3), output uncertainty is transformed into input uncertainty.

Unmodeled modes, usually (but not necessarily) occurring at high frequencies, can be handled by adjusting the norm bound on the factor uncertainty (though not necessarily at high frequencies only). This can be done iteratively: Design a controller using the technique discussed in this paper and test it on a set of perturbed full-order evaluation models. If all closed loops are stable (while achieving some desired performance level in the robust performance case), stop—the controller is satisfactory. If not, increase the norm bound on factor uncertainty and redesign the controller.

Perturbations of the coprime factors resulting from perturbations of the real parameters only are easily computed: The perturbed factor $\tilde{\boldsymbol{M}}_{rp}$ is defined as

$$\tilde{\boldsymbol{M}}_{rp} := \tilde{\boldsymbol{M}} + \Delta\boldsymbol{M}_{rp}, \tag{14}$$

where

$$\Delta\boldsymbol{M}_{rp} := \operatorname{diag}\left\{0,0,0,\frac{[2\zeta_4\delta\omega_4 + 2\delta\zeta_4(\omega_4+\delta\omega_4)]s + 2\omega_4\delta\omega_4 + \delta\omega_4^2}{s^2+as+b},\ldots,\right.$$
$$\left.\frac{[2\zeta_n\delta\omega_n + 2\delta\zeta_n(\omega_n+\delta\omega_n)]s + 2\omega_n\delta\omega_n + \delta\omega_n^2}{s^2+as+b}\right\}, \tag{15}$$

and the perturbed factor $\tilde{\boldsymbol{N}}_{rp}$ is defined as

$$\tilde{\boldsymbol{N}}_{rp} := \tilde{\boldsymbol{N}} + \Delta \boldsymbol{N}_{rp}, \tag{16}$$

where

$$\Delta \boldsymbol{N}_{rp} := \frac{\Delta B_1}{s^2 + as + b}, \tag{17}$$

Now let us consider closed-loop stability of the system in Figure 2, where a controller $\boldsymbol{K}$ is connected as a feedback around a perturbed LCF, with $\boldsymbol{U}$ and $\boldsymbol{V}$ arbitrary transfer matrices such that no pole-zero cancellation occurs in $\overline{\mathbb{C}}_+$ when the product $\boldsymbol{V}(\tilde{\boldsymbol{M}}+\Delta \boldsymbol{M})^{-1}(\tilde{\boldsymbol{N}}+\Delta \boldsymbol{N})\boldsymbol{U}$ is formed. Define the uncertainty matrix

$$\boldsymbol{\Delta} := [\Delta \boldsymbol{N} \ -\Delta \boldsymbol{M}] \ . \tag{18}$$

Clearly, if $\Delta \boldsymbol{M}_{rp}$ and $\Delta \boldsymbol{N}_{rp}$ are substituted in (18), the resulting $\boldsymbol{\Delta}_{rp}$ belongs to $\mathcal{RH}_\infty$. This matrix is defined because the result on stability of the feedback system in Figure 2 is expressed in terms of a norm bound on $\boldsymbol{\Delta}(j\omega)$ ([21], [26]). Define the uncertainty set

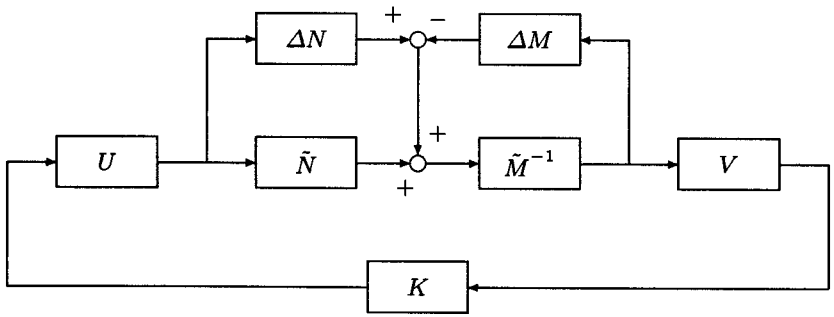

Fig. 2. Feedback control of a perturbed LCF model.

$$\mathcal{D}_r := \{\boldsymbol{\Delta} \in \mathcal{RH}_\infty \mid \|\boldsymbol{r}^{-1}\boldsymbol{\Delta}\|_\infty < 1\}, \tag{19}$$

where $\boldsymbol{r}$ is a unit in $\mathcal{H}_\infty$. The small-gain theorem yields the following slightly modified result of [26] (see also [21]).

Theorem 1. *The closed-loop system of Figure 2 with controller $\boldsymbol{K}$ is internally stable for every $\boldsymbol{\Delta} \in \mathcal{D}_r$ iff*
(a) $\boldsymbol{K}$ internally stabilizes $\boldsymbol{VGU}$, and
(b)

$$\left\| \boldsymbol{r} \begin{bmatrix} \boldsymbol{UKV}(I - \boldsymbol{GUKV})^{-1}\tilde{\boldsymbol{M}}^{-1} \\ (I - \boldsymbol{GUKV})^{-1}\tilde{\boldsymbol{M}}^{-1} \end{bmatrix} \right\|_\infty \leq 1.$$

Given the parametric uncertainty in (11), a bound of the type $|\boldsymbol{r}(j\omega)|$ that would tightly cover $\|\boldsymbol{\Delta}_{rp}(j\omega)\|$ must be found. But before this weighting function is constructed, different scalings must be performed on the factors and their perturbations to avoid any undue conservativeness and to "balance" the perturbations, i.e., to minimize the difference between the ∞-norms of $\Delta\boldsymbol{N}_{rp}$ and $\Delta\boldsymbol{M}_{rp}$. The first scaling aims at making the components of the rows and columns of B_1 have the same order of magnitude.

Let β_j denote the ∞-norm of the j^{th} column of B_1 and form

$$J_2 := \text{diag}\{\beta_1, \ldots, \beta_m\}.$$

Now let α_i denote the ∞-norm of the i^{th} row of $B_1 J_2^{-1}$ and form

$$J_1 := \text{diag}\{\alpha_1, \ldots, \alpha_n\}.$$

Let $\gamma := \|J_1^{-1} L_B J_2^{-1}\|$ and define the scaled matrices $B_{sc} := \gamma^{-1} J_1^{-1} B_1 J_2^{-1}$ and $\Delta B_{sc} := \gamma^{-1} J_1^{-1} \Delta B_1 J_2^{-1}$. For all ΔB_1 satisfying the inequalities in (11), $\|\Delta B_{sc}\| \leq 1$. Finally, we can define the scaled factor and its perturbation:

$$\tilde{\boldsymbol{N}}_0 := b\gamma^{-1} J_1^{-1} \tilde{\boldsymbol{N}} J_2^{-1} = \frac{bB_{sc}}{s^2 + as + b},$$

$$\Delta\boldsymbol{N}_{rp0} := b\gamma^{-1} J_1^{-1} \Delta\boldsymbol{N}_{rp} J_2^{-1} = \frac{b\Delta B_{sc}}{s^2 + as + b}.$$

The second scaling is performed on $\tilde{\boldsymbol{M}}$ to make sure that the norm of any perturbation of it induced by variations in the modal parameters is less than or equal to one, but close to one at low frequencies. Let $c_i := 2\zeta_i l_\omega^i + 2l_\zeta^i(\omega_i + l_\omega^i)$ and $d_i := 2\omega_i l_\omega^i + l_\omega^{i2}$ for $i = 4, \ldots, n$. These constants are the coefficients of the numerator of the (i,i) entry of $\Delta\boldsymbol{M}_{rp}$ when all modal perturbations are replaced by their upper bounds. Defining $c_{max} := \max_{i=4,\ldots,n} c_i$ and $d_{max} := \max_{i=4,\ldots,n} d_i$, we can now define the second scaled factor and its perturbation:

$$\tilde{\boldsymbol{M}}_0 := \frac{b}{d_{max}} \tilde{\boldsymbol{M}}, \quad \Delta\boldsymbol{M}_{rp0} := \frac{b}{d_{max}} \Delta\boldsymbol{M}_{rp}.$$

These two scalings are best illustrated by a sequence of block diagrams, Figure 3, showing the transformations performed on the coprime factors and their perturbations. We have included a block for the diagonal transfer matrix $\boldsymbol{T}_a$ that models actuator dynamics. Note that the properties of linearity and commutativity of diagonal matrices are used in order to move blocks around and get the desired final block diagram.

It is easy to check that $\tilde{\boldsymbol{N}}_0$ and $\tilde{\boldsymbol{M}}_0$ are still coprime and that they form an LCF of $\boldsymbol{G}_0 := d_{max}\gamma^{-1} J_1^{-1} \boldsymbol{G} J_2^{-1}$. It is our experience that these types of scalings help a lot in reducing the $\mathcal{H}_\infty$ norm of the generalized plant's weighted transfer matrix in an actual design. The last scaling performed on the perturbation $\boldsymbol{\Delta}_{rp0} := [\Delta\boldsymbol{N}_{rp0} \; -\Delta\boldsymbol{M}_{rp0}]$ normalizes it with the weighting function $\boldsymbol{r}(s)$ to get $\|\hat{\boldsymbol{\Delta}}_{rp0}\|_\infty < 1$. This is illustrated in Figure 4.

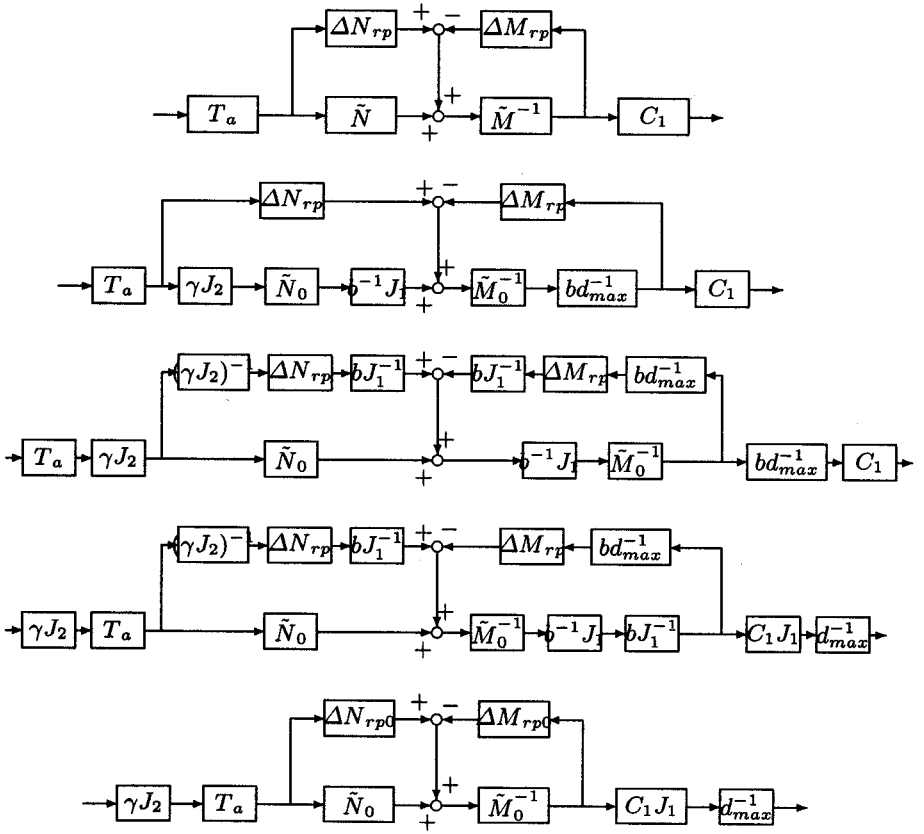

γJ_2 and d_{max}^{-1} may be absorbed by the controller.

Fig. 3. Sequence of transformations applied to the perturbed factors.

We are now ready to design a weighting function $\boldsymbol{R} = \boldsymbol{r}I$ for the scaled perturbation $\boldsymbol{\Delta}_{rp0}$. In so doing, the freedom provided by coefficients of the common denominator $s^2 + as + b$ will be used to advantage to keep the order of $\boldsymbol{r}$ as low as possible without paying the price of added conservativeness. Here is the result.

Theorem 2. *For $k > 0$, define a and b via* $s^2 + as + b := \left(s + \frac{d_{max}}{c_{max}}\right)(s + k)$

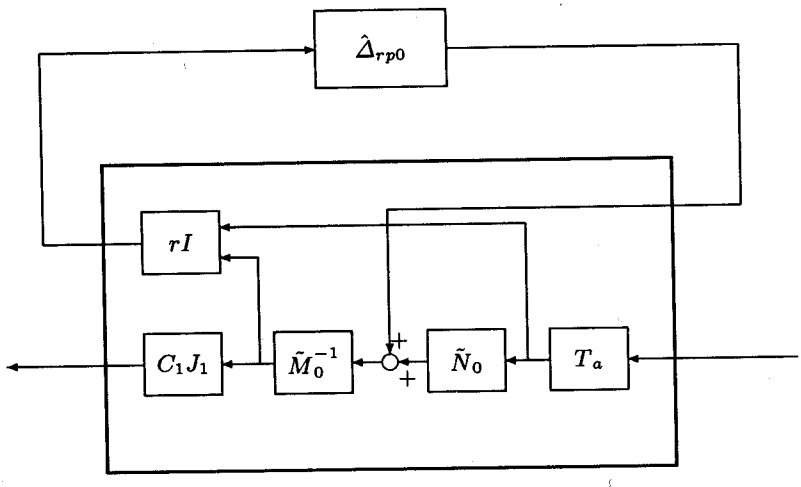

Fig. 4. Perturbed factorization after all three scalings.

and let the unit weighting function $\boldsymbol{r}$ *be given by* $\boldsymbol{r}(s) = \dfrac{\epsilon_1 s + \sqrt{2} + \epsilon_0}{(s/k+1)}$, *where* ϵ_0 *and* ϵ_1 *are small positive numbers. Then* $\|\boldsymbol{r}^{-1}\boldsymbol{\Delta}_{rp0}\|_\infty < 1$.

This weighting function is of first order, which is a benefit considering that it will be duplicated $m+n$ times in the generalized plant of Figure 5. By construction, for small ϵ_0, ϵ_1, $|\boldsymbol{r}(j\omega)|$ is a relatively tight bound on $\|\boldsymbol{\Delta}_{rp0}(j\omega)\|$, especially at low and high frequencies.

With the unit $\boldsymbol{r}$ given by Theorem 2, the factor perturbation $\boldsymbol{\Delta}_{rp0}$ belongs to the uncertainty set $\mathcal{D}_r$ and the normalized $\hat{\boldsymbol{\Delta}}_{rp0}$ belongs to $\mathcal{BRH}_\infty^{n\times(m+n)}$. Now introduce a normalized scaled perturbation $\hat{\boldsymbol{\Delta}}_0 \in \mathcal{BRH}_\infty^{n\times(m+n)}$. Then letting $\boldsymbol{\Delta}_0 := \boldsymbol{r}\hat{\boldsymbol{\Delta}}_0$, one obtains that $\boldsymbol{\Delta}_0$ is a free perturbation in $\mathcal{RH}_\infty^{n\times(m+n)}$ with $\|\boldsymbol{\Delta}_0(j\omega)\| < |\boldsymbol{r}(j\omega)|$, $\forall\omega \in \mathbb{R}$, i.e., $\boldsymbol{\Delta}_0$ is an arbitrary element in $\mathcal{D}_r$. In this way $\boldsymbol{r}$ can be included in the generalized plants of Figures 4 and 5. Figure 5 shows the scaled closed-loop system with all the weights for designing a controller $\boldsymbol{K}$ providing robust stability and nominal performance. Notice that the control input is u_{sc}, a scaled version of u. This block diagram and the associated control design problem will be discussed in the next section. According to Theorem 1, our robust stability objective will be to minimize the ∞-norm of the map $w \mapsto z_1$ to a value no more than 1 over all stabilizing controllers.

5 Robust $\mathcal{H}_\infty$ Design

Consider first the problems of attitude regulation and vibration attenuation. For these problems, it makes sense to ask for good torque/force disturbance

rejection at low frequencies as a first requirement for nominal performance. For example, this may be required on a flexible space station on which there may be large robots or humans producing significant torque disturbances. As a second requirement for nominal performance, we will ask for good tracking of reference angle trajectories to allow accurate slewing maneuvers of the rigid part of the structure. These requirements can be translated into desired shapes for the norms of the sensitivity functions $\boldsymbol{S}_{rh} := r \mapsto e_h$ and $\boldsymbol{S}_{dh} := d \mapsto y_h$, where r is the vector of input references, e_h is the vector of attitude angle errors for the rigid part of the structure (the h subscript stands for *hub*, the rigid part of Daisy), d is the vector of external torque/force disturbances, and $y_h = [\theta_{hx}\ \theta_{hy}\ \theta_{hz}]^T$ is the vector of attitude angles of the rigid part. Note that if we define $\boldsymbol{S}_r := r \mapsto e$, where e is the vector of all position/angle errors, and $\boldsymbol{S}_d := d \mapsto y$, then $\boldsymbol{S}_{rh} = \left[I_{3\times 3}\ 0_{3\times(p-3)}\right] \boldsymbol{S}_r$ and $\boldsymbol{S}_{dh} = \left[I_{3\times 3}\ 0_{3\times(p-3)}\right] \boldsymbol{S}_d$. These frequency-domain specifications are well-suited for the $\mathcal{H}_\infty$ design method (see e.g. [10]) or a μ-synthesis [2]. Here we discuss the $\mathcal{H}_\infty$ approach.

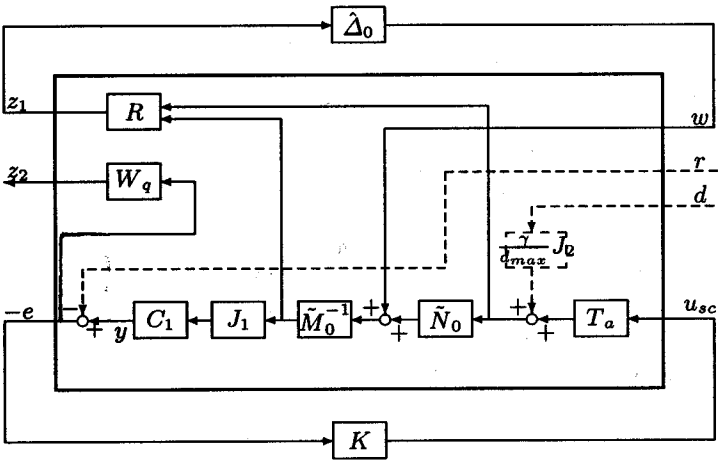

Fig. 5. Generalized plant with scaled perturbation and controller for $\mathcal{H}_\infty$ design.

The block diagram of Figure 5 shows the interconnections between the scaled factors and their perturbations, actuator dynamics, scaling and output matrices, controller, and weighting functions that form the controlled perturbed generalized plant used in the $\mathcal{H}_\infty$ design. The weighting function $\boldsymbol{W}_q$, taken to be of the form $\boldsymbol{W}_q := q\boldsymbol{w}\left[I_{3\times 3}\ 0_{3\times(p-3)}\right]$, where $q > 0$, will allow us to shape the sensitivity functions as desired. Note that the signals w, z_1, and z_2 do not have physical interpretations, but r, d and e do, as previously defined. The input

signal u_{sc} is just a scaled version of the physical signal u: $u_{sc} := \frac{\gamma}{d_{max}} J_2 u$.

In terms of Figure 5, we consider the design problem

> Design a finite-dimensional, proper, linear time-invariant controller $\boldsymbol{K}$ such that for $\hat{\boldsymbol{\Delta}}_0 \equiv 0$, the nominal closed loop of Figure 5 achieves $\|w \mapsto z\|_\infty \leq 1$.

A solution to this achieves robust stability and nominal performance in the following sense.

Theorem 3. *Assume C_1 is right invertible and let $C_1^\dagger$ be a right inverse of C_1. Let $q = \max\left\{\|\tilde{M}_0 J_1^{-1} C_1^\dagger\|_\infty,\ d_{max}^{-1}\|J_1^{-1} B_1\|\right\}$. If the controller $\boldsymbol{K}$ is internally stabilizing and achieves*

$$\left\| w \mapsto \begin{bmatrix} z_1 \\ z_2 \end{bmatrix} \right\|_\infty \leq 1, \tag{20}$$

then the closed-loop system of Figure 5 is robustly stable to all perturbations $\hat{\boldsymbol{\Delta}}_0 \in \mathcal{BRH}_\infty^{n\times(m+n)}$, and for every $\omega \in \mathbb{R}$ we have

$$\|\boldsymbol{S}_{dh}(j\omega)\| \leq |\boldsymbol{w}^{-1}(j\omega)|, \tag{21}$$

$$\|\boldsymbol{S}_{rh}(j\omega)\| \leq |\boldsymbol{w}^{-1}(j\omega)|\ . \tag{22}$$

The choice of q in Theorem 3 may be used for a first design to get insight into the tradeoff between robustness and performance, but smaller values of q may be tried to reach a satisfactory design achieving (21) and (22).

Other forms for $\boldsymbol{W}_q$ may be used to achieve other objectives such as weighting some or all of the outputs corresponding to the flexible part of the structure. Then it is easy to see that Theorem 3 remains basically the same, and particularly the expression for q is unchanged. In our experiments with Daisy, it was found that weighting all the outputs was asking too much given the uncertainty in the model and the actuator saturation levels. Hence only the hub angles were weighted with $\boldsymbol{W}_q$ as above. In any case, the modal coordinates are weighted by $\boldsymbol{r}$ (see Figure 5), which in our experiments on Daisy resulted in sufficient vibration attenuation.

To recap, if a stabilizing $\boldsymbol{K}$ satisfying (20) has been designed, it follows that (*i*) $\boldsymbol{K}$ provides robust stability to all perturbations of the modal parameters satisfying (11) and (*ii*) $\boldsymbol{K}$ provides nominal performance in the sense that inequalities (21) and (22) hold. Note that the controller $\boldsymbol{K}_p$ to be implemented on the real system is a scaled version of $\boldsymbol{K}$, i.e., $\boldsymbol{K}_p = \frac{d_{max}}{\gamma} J_2^{-1} \boldsymbol{K}$.

6 $\mathcal{H}_\infty$ Design for Daisy

The dynamic model available for Daisy is of 46^{th} order, including 20 flexible modes with frequencies ranging from approximately 0.56 rad/s to 0.71 rad/s and damping ratios from 0.015 to 0.06. The modal parameters are listed in Table 1

with crude approximations of their uncertainties obtained simply from looking at time responses. Some of the modes are multiple. Two of the rigid-body modes are pendulous, so they can be considered as flexible modes; they both have nominal frequency 0.29 rad/s and their nominal damping ratios are 0.11 and 0.09. The model has the form of (3). The method described in Section 5 is illustrated by designing a robust controller for colocated and non-colocated configurations of Daisy using the $\mathcal{H}_\infty$ design method.

mode i	frequency ω_i (rad/s)	damping ratio ζ_i
1 (rigid)	0	0
2 (rigid)	$0.286 \pm 10\%$	$0.11 \pm 50\%$
3 (rigid)	$0.293 \pm 10\%$	$0.09 \pm 50\%$
4 (flex.)	$0.568 \pm 10\%$	$0.025 \pm 50\%$
5 (flex.)	$0.568 \pm 10\%$	$0.02 \pm 50\%$
6 (flex.)	$0.569 \pm 10\%$	$0.03 \pm 50\%$
7 (flex.)	$0.569 \pm 10\%$	$0.02 \pm 50\%$
8 (flex.)	$0.569 \pm 10\%$	$0.035 \pm 50\%$
9 (flex.)	$0.569 \pm 10\%$	$0.025 \pm 50\%$
10 (flex.)	$0.569 \pm 10\%$	$0.02 \pm 50\%$
11 (flex.)	$0.572 \pm 10\%$	$0.02 \pm 50\%$
12 (flex.)	$0.592 \pm 10\%$	$0.06 \pm 50\%$
13 (flex.)	$0.593 \pm 10\%$	$0.06 \pm 50\%$
14 (flex.)	$0.657 \pm 10\%$	$0.015 \pm 50\%$
15 (flex.)	$0.657 \pm 10\%$	$0.015 \pm 50\%$
16 (flex.)	$0.657 \pm 10\%$	$0.02 \pm 50\%$
17 (flex.)	$0.657 \pm 10\%$	$0.02 \pm 50\%$
18 (flex.)	$0.657 \pm 10\%$	$0.027 \pm 50\%$
19 (flex.)	$0.657 \pm 10\%$	$0.025 \pm 50\%$
20 (flex.)	$0.657 \pm 10\%$	$0.02 \pm 50\%$
21 (flex.)	$0.670 \pm 10\%$	$0.04 \pm 50\%$
22 (flex.)	$0.672 \pm 10\%$	$0.05 \pm 50\%$
23 (flex.)	$0.714 \pm 10\%$	$0.015 \pm 50\%$

Table 1. Modal parameters of Daisy's model.

Here we consider only colocation, by which we mean that all rotations and displacements produced by the actuators at their locations are measured. Thus 23 actuator/sensor pairs are used, namely the 20 bidirectional rib thrusters with the DEOPS system measuring the 20 rib angles, plus the three hub reaction wheels with the three corresponding angle encoders. In terms of system equations (3) and (4), the inputs are $u = [\tau_{hx}\, \tau_{hy}\, \tau_{hz}\, \tau_{r1}\, \tau_{r2} \cdots \tau_{r20}]^T$, where the first three are the hub torques around the x, y and z axes, and the last twenty inputs are the rib torques given by

$$\tau_{ri} = \begin{cases} \text{rib } (i+1)/2 \text{ out-of-cone torque}, & i \text{ odd}, \\ \text{rib } i/2 \text{ in-cone torque}, & i \text{ even}. \end{cases} \tag{23}$$

All torque inputs are expressed in Nm. The input matrix $B_1 \in \mathbb{R}^{23\times 23}$ is assumed to have up to 8% uncertainty in its entries. Note that the torque wheels have some dynamics, i.e., for each wheel, the transfer function between the desired and produced torques is first-order and strictly proper. On the other hand, the PWM thrusters, which deliver average torques close to the desired ones, are modeled as pure gains. Overall, the transfer matrix $\boldsymbol{T}_a$ in Figure 5 is taken to be

$$\boldsymbol{T}_a = \text{diag}\left\{\frac{0.01s+1}{0.36s+1}, \frac{0.01s+1}{0.36s+1}, \frac{0.01s+1}{0.36s+1}, 1, 1, \ldots, 1\right\}, \tag{24}$$

where the the terms $0.01s$ are added in the numerators to regularize the generalized plant for the $\mathcal{H}_\infty$ problem, and the 0.36 time constants were measured experimentally. Note that $\boldsymbol{T}_a$ commutes with J_2. The outputs are the angles $y = [\theta_{hx}\theta_{hy}\theta_{hz}\theta_{r1}\theta_{r2}\cdots\theta_{r20}]^T$, which correspond to the input torques described above. The output matrix is just the mode shape matrix $C_1 = E \in \mathbb{R}^{23\times 23}$, which is invertible. All angles are expressed in radians. Finally, $\Lambda = \text{diag}\{\omega_1^2, \ldots, \omega_{23}^2\}$ and $D = \text{diag}\{2\zeta_1\omega_1, \ldots, 2\zeta_{23}\omega_{23}\}$, where the modal parameters are those given in Table 1. A plot of the 23 singular values of $C_1\boldsymbol{G}(j\omega)$ is shown in Figure 6. It turns out that all the modes are significant and as a result it is very difficult to reduce the number of modes in the model. This was concluded from an analysis of the Hankel singular values of a normalized coprime factorization of the plant model $C_1\boldsymbol{G}$ [22]: They all lie between 0.2 and 0.9, which indicates that the model should not be reduced. Consequently, our design model includes all the modes in Table 1. It should be noted that this method of characterizing the input/output influence of the modes in the model seems appropriate for our control design method based on a coprime factorization. It avoids the singularity of measures such as modal costs [24] and Hankel singular values of the plant [12] when the damping ratios go to zero.

It is desired to control Daisy's model so that it remains stable for all bounded perturbations of the modal parameters in Table 1 and all perturbations of the entries of B_1 within 8% of their nominal values. We also want good torque/force disturbance rejection and good tracking in the sense of (21) and (22). The diagonal scaling matrices J_1 and J_2 are computed as explained in Section 4. The constants and weighting functions are

$$d_{max} = 0.107, \quad c_{max} = 0.046, \quad k = \frac{c_{max}}{d_{max}} = 0.43, \quad \gamma = 0.79, \quad q = 1000,$$

$$\boldsymbol{w}(s) = \frac{100}{s^2/(0.01)^2 + 2\times 0.7s/0.01 + 1}, \tag{25}$$

$$\boldsymbol{r}(s) = \frac{0.001s + 1.415}{2.33s + 1}. \tag{26}$$

Computational delay and zero-order hold models were not included in the generalized plant even though both were present in the digital implementation of the controller on Daisy. It was anticipated that the design would be robust to these unmodeled dynamics; this was borne out by experiments. No antialiasing analog filters were available to filter the measured hub angle signals, nor

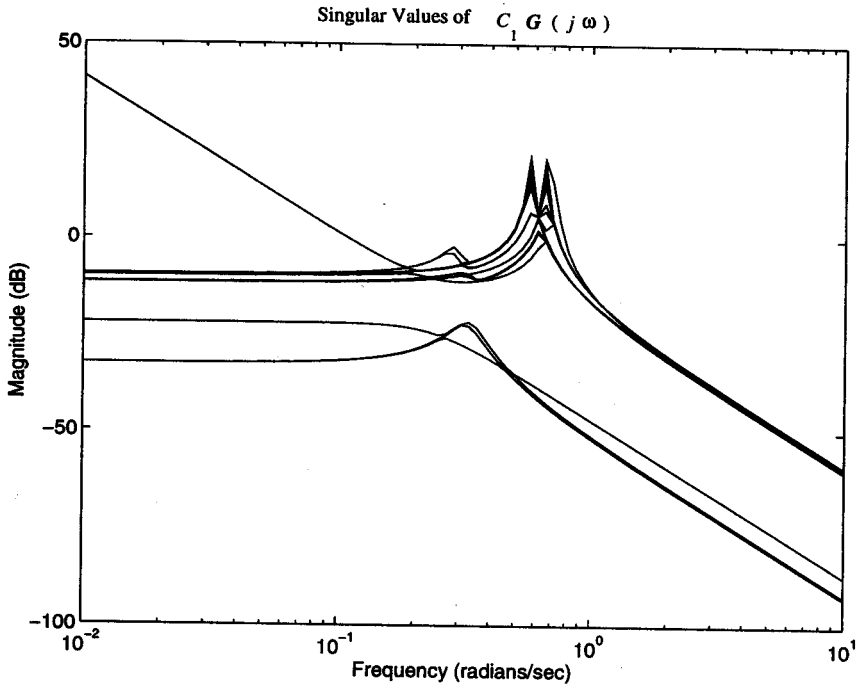

Fig. 6. Singular values of $C_1 G(j\omega)$.

for DEOPS signals, which are inherently digital. Even though this is rather undesirable, high-frequency noise levels seemed sufficiently small to avoid serious aliasing problems in the experiments. The $\mathcal{H}_\infty$ design was carried out in MATLAB^{TM} using the μ-Tools^{TM} [2] command *hinfsyn*. If a realization of the generalized plant is obtained using a computer, it will in general be nonminimal because pole-zero cancellations might not be carried out. Also note that the generalized plant is unstable, so one cannot use the balanced truncation method [23] to get rid of the unobservable and uncontrollable modes. Therefore we used the decentralized fixed-mode method [9] to obtain a minimal realization, reducing it from 147 to 78 state variables, which equals its McMillan degree. This method has the advantage of being computationally simple and hence more reliable for such large systems.

A stable suboptimal controller achieving $\|w \mapsto z\|_\infty = 0.94$ was obtained. Its order was the same as the order of the minimal generalized plant, i.e., 78, but a balanced truncation reduced it to 55 state variables without affecting the closed-loop ∞-norm. With this reduced controller $\boldsymbol{K}_1$, Figure 7 shows that required performance has been attained, i.e., $\|\boldsymbol{S}_{rh}(j\omega)\|$ and $\|\boldsymbol{S}_{dh}(j\omega)\|$ are less than $|\boldsymbol{w}^{-1}(j\omega)|$, as desired. The least-damped closed-loop mode has a damping

ratio of 0.38.

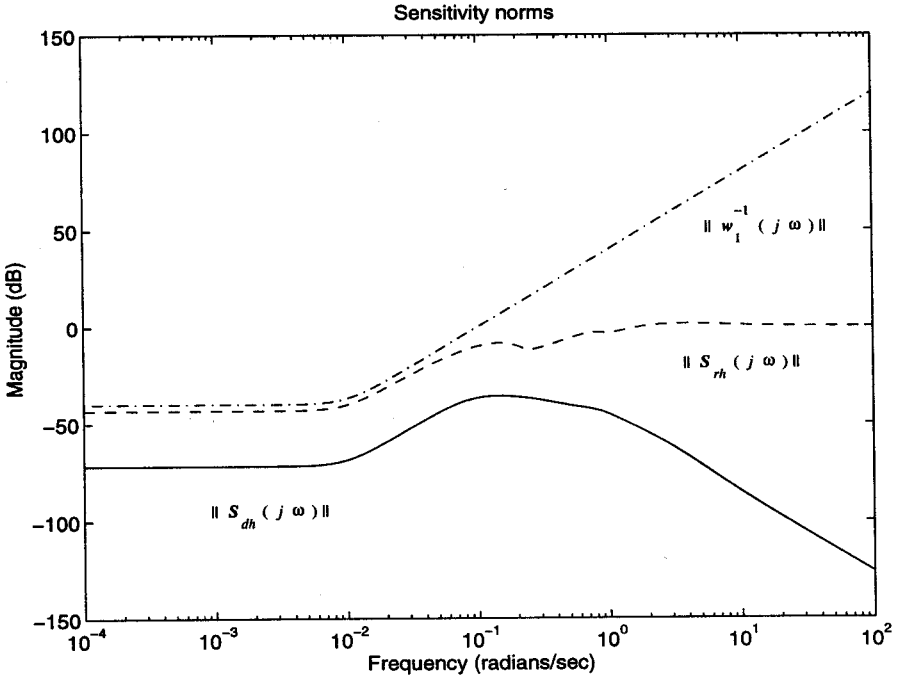

Fig. 7. Norms of $S_{dh}(j\omega)$ and $S_{rh}(j\omega)$ for K_1.

The 55^{th}-order controller $\boldsymbol{K}_1$ was rescaled to $\boldsymbol{K}_{p1} = \frac{d_{max}}{\gamma} J_2^{-1} \boldsymbol{K}_1$, a controller using the actual rib and hub angles to compute actual rib and hub control torques. Then, since the implementation of the controller must be digital, $\boldsymbol{K}_{p1}$ was discretized at a sampling rate of 10 Hz using the bilinear transformation; call the resulting controller $\boldsymbol{K}_{p1d}$. Another discretized version of the controller was computed using the MATLAB^{TM} function *c2d*—it destabilized Daisy both in simulations and experiments. The *c2d* function performs the discretization by placing a sampler at the output of the controller and a zero-order hold at the input. The frequency responses of $\boldsymbol{K}_{p1}$ and $\boldsymbol{K}_{p1d}$ were close up to 10 rad/s, whereas for the controller discretized with *c2d*, the frequency responses started to differ significantly from 1 rad/s. The 10 Hz sampling rate was almost the highest achievable on the real-time control computer system with our control software. An earlier version of the program allowed a maximum sampling rate of 5 Hz only—when used to implement a discretized version of $\boldsymbol{K}_{p1}$, it destabilized the closed loop. This suggests that an $\mathcal{H}_\infty$-optimal sampled-data design might be warranted here, but this is left for future work.

We used the following hub torque disturbance profile for all tests:

$$\begin{cases} A_d, & \text{if } 0 \leq \mathrm{t} \leq \mathrm{T} \\ -1.5A_d, & \text{if } \mathrm{T} < \mathrm{t} \leq 2\mathrm{T} \\ 0, & \text{else.} \end{cases}$$

It can be applied by any of the three torque wheels, individually or in any combination. Notice that this disturbance is completely specified by three parameters: the amplitude of the first torque pulse, A_d; the duration of the first and second pulses, T; and the combination of hub axes around which the disturbance is applied, *axes*. This latter parameter can take on values in the set $\{x, y, z, xy, xz, yz, xyz\}$. With these definitions, let us denote the disturbance as $D(A_d, T, axes)$. The controller is switched on after the hub angle experiencing the largest deviation changes sign. Thus the disturbance has roughly the effect of a torque impulse applied to the hub because the controller starts when the hub angles are small while the angular velocities are large. However, the rib angles may not be small at switch-on time. Although experimental controller performance would be best assessed by performing frequency-response experiments and comparing with $\boldsymbol{S}_{dh}(j\omega)$, these are certainly not practical for LFSSs. But the torque impulse response matrix is just the inverse Laplace transform of the sensitivity $\boldsymbol{S}_d$. Hence this provides some motivation for judging and comparing controller performance using time responses of the rib and hub angles to the disturbance $D(A_d, T, axes)$. For all the plots, $t = 0$ corresponds to the instant at which the controller is turned on.

As a benchmark, an open-loop response of Daisy to $D(13.5\mathrm{Nm}, 2s, x)$ is plotted in Figure 8 along with a simulated continuous-time response of the nominal model $C_1\boldsymbol{G}$. Discrepancies between some of the actual and nominal modal frequencies and damping ratios can be observed from these plots, illustrating the uncertainty in the model.

All simulations are linear and *discrete-time* with the plant model (including actuator dynamics) discretized at 10 Hz using *c2d*. As a typical test run, for the torque disturbance $D(13.5\mathrm{Nm}, 2s, y)$, Figures 9 and 10 show respectively the hub and rib angle responses, while the hub control torques are plotted in Figure 11 and the rib control torques are in Figure 12. When compared with the response in Figure 8, it is clear that the $\mathcal{H}_\infty$ controller vastly improves the dynamics of Daisy. The experimental response of θ_{hy} has a slightly longer settling time than its simulated counterpart. The rib responses are quite consistent with the simulated ones, showing actual performance very close to the nominal. This is in spite of rib torque saturation, which occurred for the first two seconds.

In conclusion, the experimental data show that the $\mathcal{H}_\infty$ controller $\boldsymbol{K}_{p1d}$ designed using the coprime factorization method performed quite well. *No experimental tuning of the controller was necessary*, which shows evidence of robustness of the design.

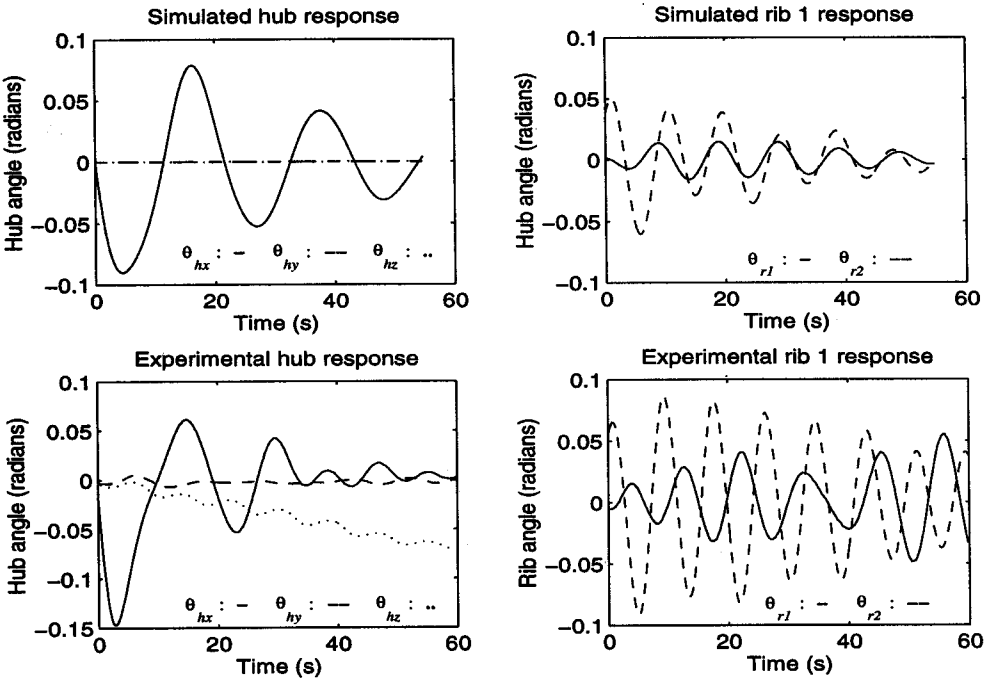

Fig. 8. Simulated and experimental open-loop responses of Daisy to $D(13.5\text{Nm}, 2s, x)$.

7 Conclusion

A new approach introduced in [3] to the robust control of LFSSs using a coprime factor description of the plant's dynamics was presented. This approach first involves the transformation of a natural description of the uncertainty as bounded perturbations of the modal parameters of an original FE model into norm-bounded stable perturbations of a nominal coprime factor pair. This new unstructured description of the uncertainty is not overly conservative in terms of real perturbations of the modal parameters, and it can also represent unmodeled dynamics. Moreover, the $\mathcal{H}_\infty$ and μ-synthesis controller design methods can be used with this type of uncertainty, and lead to computationally tractable problems despite the high order of LFSS dynamics. To illustrate the technique, an $\mathcal{H}_\infty$ controller was designed for Daisy. This model has significant parameter uncertainty, yet the controller designed using the coprime factorization technique was quite robust and achieved good performance levels in terms of rejection of hub torque disturbances. Furthermore, the controllers were stable, which is a desirable property. Extensive experimentations showed that digital implementations of the $\mathcal{H}_\infty$ controller performed very well without the need of any experimental tuning. Further work is underway to include nonlinearities and sampling issues

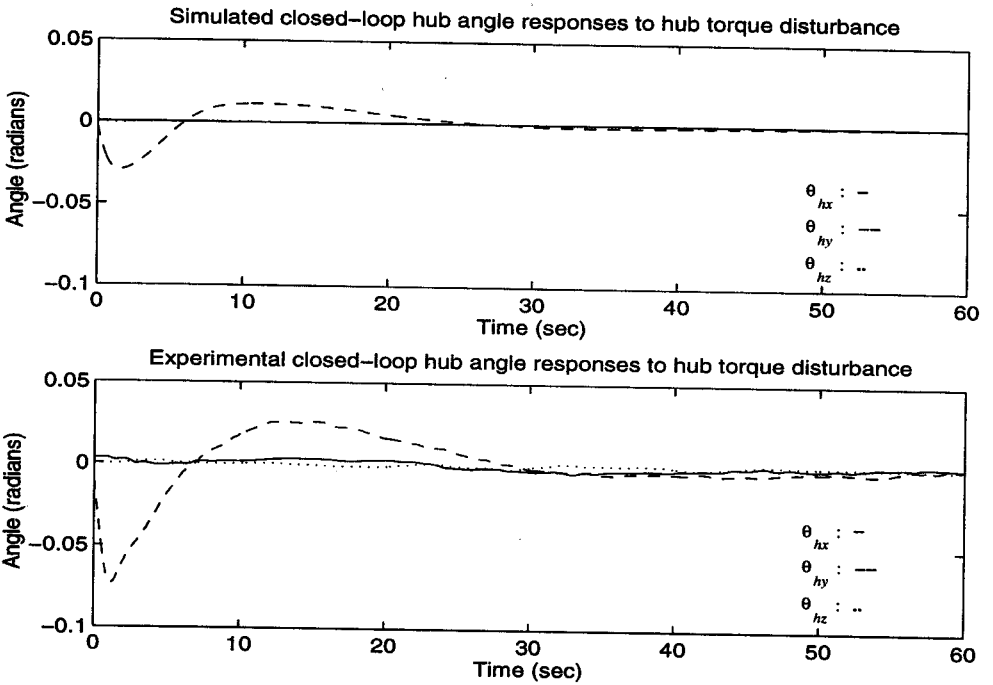

Fig. 9. Simulated and experimental closed-loop hub angle responses with K_{p1d}, $D(13.5\text{Nm}, 2s, y)$.

into the design technique.

8 Acknowledgements

Much thanks to Vince Pugliese, system manager, and Regina Sun Kyung Lee, graduate student, both from UTIAS, for help with the experiments. Regina also provided the drawing of Daisy in Figure 1.

References

1. G.J. Balas and J.C. Doyle, Robustness and Performance Tradeoffs in Control Design for Flexible Structures. *Proc. of the 1991 Amer. Control Conf.*
2. G.J. Balas, J.C. Doyle, K. Glover, A. Packard, and R. Smith, *μ-Analysis and Synthesis Toolbox: User's Guide.* The Mathworks Inc., 1991.
3. B. Boulet, B.A. Francis, P.C. Hughes, and T. Hong, Robust control of large flexible space structures using a coprime factor plant description. Proc. of the 1994 Amer. Cont. Conf., Baltimore, Maryland, pp. 265-266.

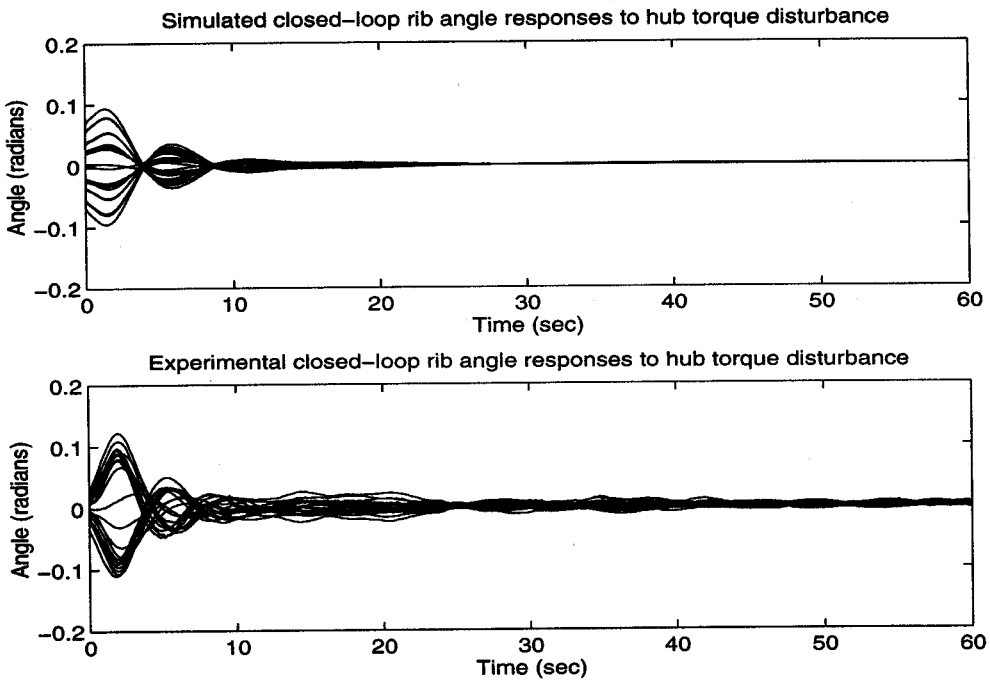

Fig. 10. Simulated and experimental closed-loop rib angle responses with K_{pid}, $D(13.5\text{Nm}, 2s, y)$.

4. B. Boulet, B.A. Francis, P.C. Hughes, and T. Hong, Robust $\mathcal{H}_\infty$ Control of Large Flexible Space Structures Using a Coprime Factor Plant Description. *Systems Control Group Report No. 9401*, Dept. of Electrical and Computer Engineering, University of Toronto, 1994.
5. R.P. Braatz, P.M. Young, J.C. Doyle, and M. Morari, Computational Complexity of μ Calculation. *IEEE Trans. Aut. Control, Vol. 39, No. 5, pp. 1000-1002, May 1994.*
6. S.A. Buddie, T.T. Georgiou, U. Özgüner, and M.C. Smith, Flexible structure experiment at JPL and WPAFB: $\mathcal{H}_\infty$ controller designs. *Int. J. Control, Vol. 58, No. 1, pp. 1-19, 1993.*
7. E.G. Collins, Jr., D.J. Phillips, and D.C. Hyland, Robust Decentralized Control Laws for the ACES Structure. *IEEE Control Syst. Magazine, Vol. 11, No. 3, pp. 62-70, April 1991.*
8. G.W. Crocker, P.C. Hughes, and T. Hong, Real-Time Computer Control of a Flexible Spacecraft Emulator. *IEEE Control Syst. Magazine, Vol. 10, No. 1, pp. 3-8, January 1990.*
9. E.J. Davison, W. Gesing, and S.H. Wang, An Algorithm for Obtaining the Minimal Realization of a Linear Time-Invariant System and Determining if a System is Stabilizable-Detectable. *IEEE Trans. Aut. Control, Vol. 23, No. 6, pp. 1048-1054,*

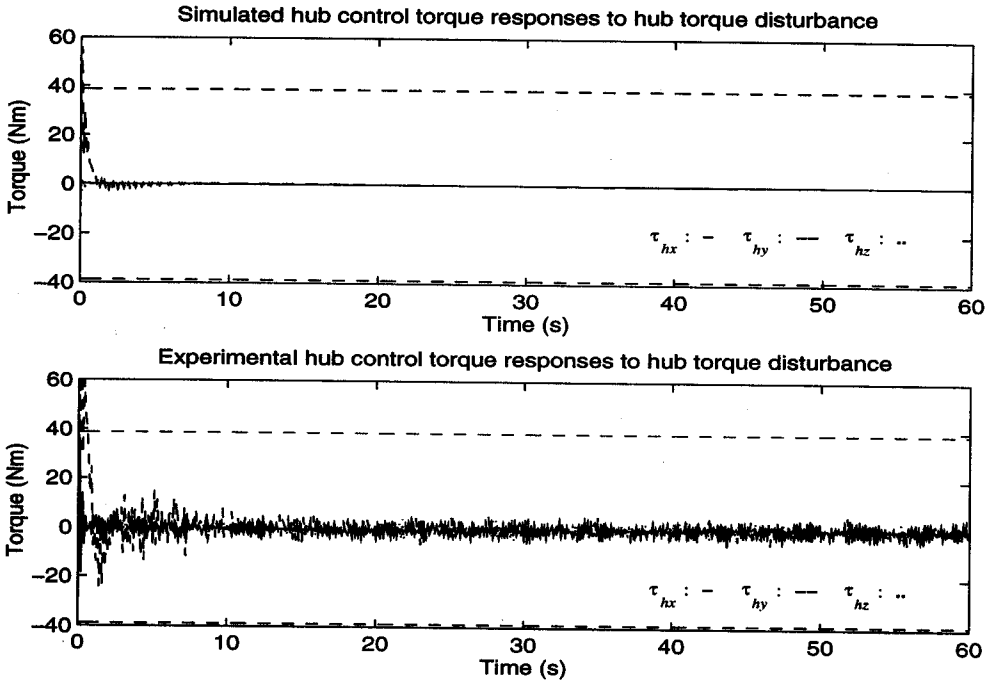

Fig. 11. Simulated and experimental computed hub control torques for K_{p1d}, $D(13.5\text{Nm}, 2s, y)$.

December 1978.

10. J.C. Doyle, K. Glover, P.P. Khargonekar, and B.A. Francis, State-Space Solutions to Standard $\mathcal{H}_2$ and $\mathcal{H}_\infty$ Control Problems. *IEEE Trans. Aut. Control, Vol. 34, No. 8, pp. 831-847, August 1989.*
11. M.K.H. Fan, A.L. Tits, and J.C. Doyle, Robustness in the Presence of Mixed Parametric Uncertainty and Unmodeled Dynamics. *IEEE Trans. Aut. Control, Vol. 36, No. 1, pp. 25-38, January 1991.*
12. C.Z. Gregory, Jr., Reduction of Large Flexible Spacecraft Models Using Internal Balancing Theory. *AIAA J. of Guid., Contr. and Dyn., Vol. 7, No. 6, Nov.-Dec. 1984.*
13. R.A. Horn and C.R. Johnson, *Matrix Analysis*, Cambridge Univ. Press, 1990.
14. J.P. How, W.M. Haddad, and S.R. Hall, Robust Control Synthesis Examples with Real Parameter Uncertainty using the Popov Criterion. *Proc. of the Amer. Control Conf., San Francisco, June 1993.*
15. J.P. How, S.R. Hall, and W.M. Haddad, Robust Controllers for the Middeck Active Control Experiment using Popov Controller Synthesis. *IEEE Trans. Control Syst. Tech., Vol. 2, No. 2, pp. 73-87, June 1994.*
16. S.M. Joshi, Control of Large Flexible Space Structures. *Lecture Notes in Control and Information Sciences, Vol. 131*, New-York: Springer-Verlag, 1989.

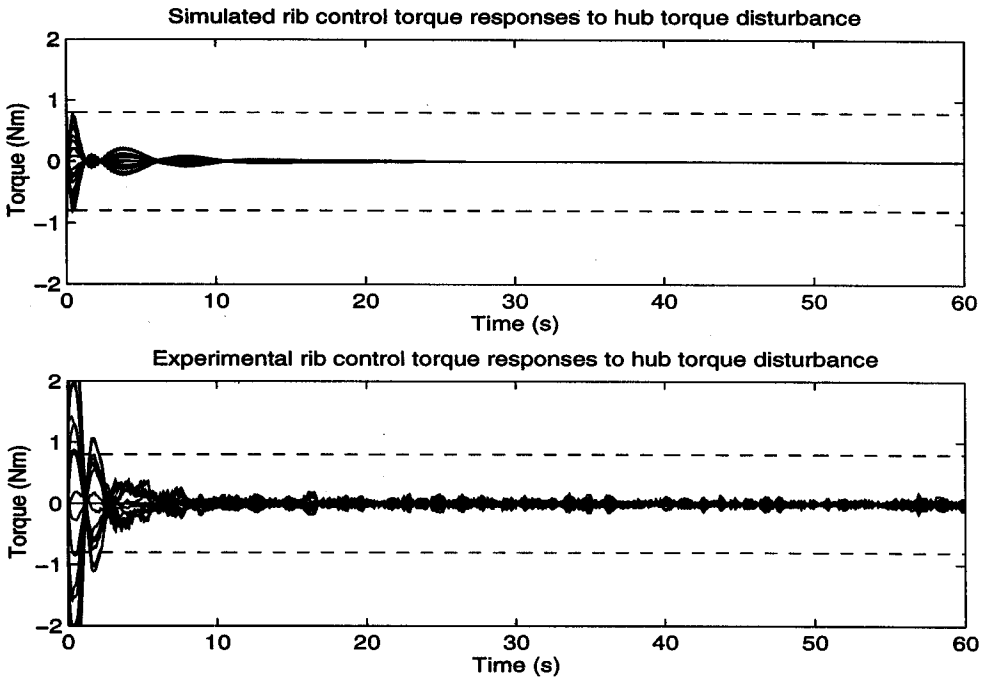

Fig. 12. Simulated and experimental computed rib control torques for K_{pid}, $D(13.5\text{Nm}, 2s, y)$.

17. D.G. Laurin, Development of an Optical Imaging System for Shape Monitoring of Large Flexible Structures. Ph.D. Thesis, Dept. of Aerospace Eng., Univ. of Toronto, 1992.
18. F.C. Lee, H. Flashner, and M.G. Safonov, Positivity Embedding for Noncolocated and Nonsquare Flexible Structures. *Proc. of the Amer. Control Conf., June 1994, Baltimore, Maryland.*
19. K.B. Lim and G.J. Balas, Line-of-sight Control of the CSI Evolutionary Model: μ Control. *Proc. of the 1992 Amer. Control Conf.*
20. K.B. Lim, P.G. Maghami, and S.M. Joshi, Comparison of Controller Designs for an Experimental Flexible Structure. *IEEE Control Syst. Magazine, Vol. 12, No. 3, pp. 108-118, June 1992.*
21. D.C. McFarlane and K. Glover, *Robust Controller Design Using Normalized Coprime Factor Plant Descriptions, Springer-Verlag, 1990.*
22. D.G. Meyer, A Fractional Approach to Model Reduction. *Proc. of the Amer. Control Conf., pp. 1041-1047, 1988, Atlanta.*
23. B.C. Moore, Principal Component Analysis in Linear Systems: Controllability, Observability, and Model Reduction. *IEEE Trans. Aut. Control, Vol. 26, No. 1, pp. 17-32, February 1981.*

24. R.E. Skelton and P.C. Hughes, Modal Cost Analysis for Linear Matrix-Second-Order Systems. *ASME J. Dyn. Syst., Meas., and Cont., Vol. 102, pp. 151-158, September 1980.*
25. R.S. Smith, C.-C. Chu, and J.L. Fanson, The Design of $\mathcal{H}_\infty$ Controllers for an Experimental Non-collocated Flexible Structure Problem. *IEEE Trans. Control Syst. Tech., Vol. 2, No. 2, pp. 101-109, June 1994.*
26. M. Vidyasagar, *Control System Synthesis: A Coprime Factorization Approach. MIT press*, 1985.